Research Article

The Effect of Various Cations/Anions for MgH_2 Hydrolysis Reaction

Chongyang Yuan [1], Wei Chen [1], Zunxian Yang [2,*], Zhenguo Huang [3], Xuebin Yu [1,*]

[1] *Department of Materials Science, Fudan University, Shanghai 200433, China*

[2] *National and Local United Engineering Laboratory of Flat Panel Display Technology, Fuzhou University, Fuzhou 350002, Fujian, China*

[3] *School of Civil & Environmental Engineering, University of Technology Sydney, Ultimo, New South Wales 2007, Australia*

[Received ; Received in revised form ; Accepted]

* Corresponding author. Prof. Yu, Prof. Yang; Tel.: 021-55664581.

E-mail address: yuxuebin@fudan.edu.cn (X. Yu); yangzunxian@hotmail.com (Z. Yang).

MgH_2 is regarded as a potential hydrolysis material for the hydrogen generation due to its high theoretical hydrogen yield, abundant source on earth and environmentally friendly hydrolysates. However, the quickly formed passive magnesium hydroxide layer on the surface of MgH_2 will hinder its further hydrolysis reaction, leading to sluggish reaction kinetics and low H_2 yield. In this paper, we explore the improvement of different anions and cations in solutions for the hydrolysis of MgH_2. It is found that the cations in the solution promote the reaction rate of MgH_2 hydrolysis through the hydrolysate-induced growth effect, among which the fastest hydrogen yield can get 1664 mL/g within a few minutes in the $Fe_2(SO_4)_3$ solution. As for the anions, it enables different microstructures of the $Mg(OH)_2$ hydrolysate which give rise to enhanced water utilization. Specially, for the mixed 0.5 M $MgCl_2$ + 0.05 M $MgSO_4$ solution, the water utilization rate attains the optimum value of 51.3%, much higher than that of the single $MgCl_2$ or $MgSO_4$ solutions. These findings are of great significance for the application of MgH_2 hydrolysis as hydrogen generation.

Key words: MgH_2; hydrolysis reaction; cations; anions; hydrogen generation

1. Introduction

To improve the ecological environment resulted from the consumption of fossil energy, new clean energy needs to be developed and implemented. Hydrogen, with the advantages of high energy density (142 MJ/kg), benign environmental compatibility, and abundant resources, is the most promising energy carrier for replacing traditional fossil fuels[1-3]. So far, it has contained great challenges for mass production, storage and controlled distribution of hydrogen which could be the critical part of the pursuit for the hydrogen economy[4].

Compared to traditional hydrogen storage methods, such as compressed gaseous hydrogen and low-temperature liquid hydrogen, solid hydrogen storage shows the advantages of high hydrogen storage volume density, high safety, low cost and so forth[5-7]. Among the solid hydrogen storage materials, MgH_2 holds the promise as an energy carrier medium due to its non-toxicity, high hydrogen content (7.6 wt.%) and low price[8,9]. What's more, because of its strong reducibility when MgH_2 reacts with water at room temperature, it will undergo a chemical reaction as shown in formula (1) and the hydrogen yield can reach to 15.2 wt. % if the weight of water is not calculated, which makes it especially suitable for the fuel cell in supplying hydrogen[10-14].

$$MgH_2 + 2H_2O = Mg(OH)_2 + 2H_2\uparrow \quad \triangle H = -277\ \text{kJ/mol} \tag{1}$$

However, $Mg(OH)_2$, which is low solubility in water, is the by-product of MgH_2 hydrolysis and it is usually formed on the surface of MgH_2. The passive $Mg(OH)_2$ layer will hinder the further contact of water with fresh MgH_2 and thus leading to sluggish hydrolysis kinetics[14,15]. A number of approaches have been proposed to solve this problem by modifying the MgH_2, involving in alloying[16,17], designing nanostructure[18-20], ball-milling with other metal hydrides[21], oxides[22], carbon additives[22], chlorides[23] or other chemicals[24]. These methods can improve hydrogen yield and hydrolysis kinetics to a certain extent.

Furthermore, changing the component of aqueous solution is another easy-operated and efficient way to promote the hydrolysis process of MgH_2. Gan et al.[25] found that a hydrogen generation of 1487 mL/g in 10 min at 303 K was achieved for the MgH_2 powder in 0.5 mol/L $AlCl_3$ solution. In addition, ammonium salts have been applied in MgH_2 hydrolysis. Huang et al.[26] reported that hydrogen generation via MgH_2 hydrolysis in 4.50 wt. % NH_4Cl solution produced 1604 mL/g hydrogen in 10 min at 333 K. Chen et al.[15] combined MgH_2 nanoparticles and $MgCl_2$ solution to promote the hydrolysis process of MgH_2 and discovered near-theoretically 1820 mL/g of H_2 released within 20 min in 1 mol/L $MgCl_2$ solution. Sevastyanova et al.[27] adopted mixed solutions of magnesium chloride with aqueous

ammonium, copper or potassium chlorides to accelerate the MgH_2 hydrolysis process and observed the highest reaction rate yielding of 100% hydrogen releasing in 120 min in mixed 0.45 mol/L $MgCl_2$ and 0.85 mol/L NH_4Cl solutions. Clearly, the promoted hydrolysis process of MgH_2 in above studies is attributed to the addition of various salts. It has been proposed by Zheng et al. that the cations of the chlorides play a critical role in the hydrolysis reaction and the cations with higher OH^- affinity are more effective for facilitating the hydrolytic reaction[28]. As for the effect of anions in the reaction, however, there has never been reported yet.

In this work, we first demonstrate that excellent H_2 generation can be achieved by reaction of MgH_2 powder with several chloride and sulfate solutions without any activation procedure, and the role of cations/anions on the improvement of MgH_2 hydrolysis is discussed. And then we put forward the concept of water utilization rate, which means the ratio of measured hydrogen production to theoretical hydrogen production of the total employed water in the MgH_2 hydrolysis reaction. Our results indicate that the mixture of $MgCl_2$ and $MgSO_4$ solution can obtain higher water utilization than that of separate $MgCl_2$ and $MgSO_4$ solutions. This study lays the foundation for the practical application of MgH_2 hydrolysis.

2. Experimental

2.1 Materials and characterizations

MgH_2 powder (Shanghai Magnesium Power, 99.0%, 500 mesh, XRD patterns are shown in Fig. S1 in supplementary material), $MgCl_2·6H_2O$, $CuCl_2·4H_2O$, $ZnCl_2$, $FeCl_3·6H_2O$, $MgSO_4·7H_2O$, $CuSO_4·5H_2O$, $ZnSO_4·7H_2O$, $Mg(NO_3)_2·6H_2O$ (Shanghai Hushi, AR) and $Fe_2(SO_4)_3$, $Mg(CH_3COO)_2·4H_2O$ (Macklin, 99.0%) and $Mg(ClO_4)_2·6H_2O$ (Aladdin, 99.99%) were used as received commercially.

X-ray diffraction (XRD) patterns are collected using the CuKα line at a scan rate of 10° min^{-1} (Rigaku D/max 2000 diffractometer). Scanning electron microscopy (SEM) images are collected with acceleration voltage of 1 kV (Hitachi S4800).

2.2 Hydrogen generation test

The hydrogen generation test system is showed in Fig. 1. The hydrolysis was carried at a 100 ml three-necked flask: one sealed with a rubber stopper, one for solution injection and

MgH_2 powder addition, the last one for the hydrogen collection and recording. For the measurement of H_2 yield, various solution (20 mL, 0.5 mol/L, hereinafter abbreviated as "M") was loaded in the flask and was kept at a certain temperature by a water bath. MgH_2 powder (0.1 g) was added into the solution under moderate stirring and the system was rapidly sealed. The generated hydrogen passes through a drier to remove the water vapor, and the volume of H_2 was recorded by a flowmeter (Ritter MGC-1 V3.4 PMMA) connected with a computer. The rubber tubes were used to connect the flask, the drier and the flowmeter. The hydrogen is exhausted to the outside to ensure safety.

It is common that the amount of H_2O is far exceeding for MgH_2 hydrolytic reaction and the H_2O utilization is low which leads to a decreased hydrogen capacity in the whole MgH_2/H_2O system. In this situation, we used the term H_2O utilization rate to describe the hydrogen capacity of the whole MgH_2/H_2O system. The H_2O utilization rate is the ratio of experimentally measured hydrogen yield to stoichiometric hydrogen yield of the total employed water in the MgH_2 hydrolysis reaction. Thus, the higher H_2O utilization rate means the higher system hydrogen capacity. For the measurement of H_2O utilization rate, 0.4 g MgH_2 powder was added in batches into 10 mL solution until the hydrogen evolution of the entire system stopped, and the data of the released H_2 was used to calculate the H_2O utilization rate.

After hydrolysis reaction, the precipitates were centrifuged and washed with water and ethanol three times and dried at 60 °C via dynamic vacuum on a Schlenk line.

3. Results and discussion

3.1. The influence of cations in MgH_2 hydrolysis

Fig. 2 shows the hydrogen generation of MgH_2 hydrolysis in different chloride and sulfate solutions with the same volume and concentration. It is obviously that the total amount of H_2 yield and the H_2 release rate have been improved greatly due to the existence of chloride/sulfate compared with the MgH_2 hydrolysis in pure water, for which only 5.0% (94.0 mL/g) theoretical H_2 is released after 2 h. The slow reaction kinetics in the case of MgH_2/pure water is caused by the formation of passivated $Mg(OH)_2$ layer on the surface of the MgH_2 particles as previous reports[29]. In Fig. 2a, it can be clearly seen that the $FeCl_3$ solution shows the highest reaction rate, releasing 1632.0 mL/g H_2 in 6.2 min. $CuCl_2$ also delivers a good activity and releases 810.3 mL/g H_2 in 20 min, while the H_2 generation for $ZnCl_2$ and $MgCl_2$ solutions is 561.2 mL/g and 491.4 mL/g, respectively. The H_2 generation data from MgH_2 in various sulfate solutions gives the analogous promoting rules as shown in Fig. 2b. What's more,

89.0% (1664.0 mL/g) theoretical H_2 is released in the $Fe_2(SO_4)_3$ solution in 5 min and the $CuSO_4$ solution provides 816.7 mL/g H_2 in 20 min. The H_2 generation after 20 min in $ZnSO_4$ solution is 378.6 mL/g, higher than that in $MgSO_4$ solution (244.5 mL/g). Hence, integrating the above cases, it can be drawn that the hydrolysis rate is enhanced in the order of Mg^{2+} < Zn^{2+} < Cu^{2+} < Fe^{3+}.

To further reveal the superb improvement of MgH_2 hydrolysis in $Fe_2(SO_4)_3$ solution, kinetic curves of hydrogen evolution from MgH_2 hydrolysis in $Fe_2(SO_4)_3$ solution as compared with in pure water were measured at different temperatures. As shown in Fig. 2c, even at a low temperature of 274 K, the MgH_2 can release 96.1% theoretical H_2 in 16 min in the $Fe_2(SO_4)_3$ solution.

The relationship between temperature and rate of MgH_2 hydrolysis can generally be expressed by the Arrhenius equation:

$$\ln k = \ln A - E_a/RT \quad (2)$$

where k is the reaction rate constant, E_a is the activation energy (J mol^{-1}), R is the gas constant (8.314 J mol^{-1} K^{-1}), and T is the reaction temperature (K). Fig. 2d presents an Arrhenius plot for the hydrolysis of the MgH_2 in $Fe_2(SO_4)_3$ solution and the activation energy (E_a) was calculated to be 19.15 kJ mol^{-1}, which is lower than that of previously reported hydrolysis of MgH_2 in $AlCl_3$ solution (21.64 kJ mol^{-1})[25] and NH_4Cl solution (30.37 kJ mol^{-1}) [26]. As for the MgH_2 hydrolysis in pure water, due to the inevitable formation of $Mg(OH)_2$ passivation layer on the surface of MgH_2 particle, the hydrogen release rate was improved at first but quickly degraded at the high temperature, leading to a very low hydrolysis efficiency, as shown in Fig. S3.

It has been reported that cations with higher OH^- affinity are more effective for facilitating the Mg hydrolytic reaction[28]. The precipitation from the metal chloride and sulfate solutions was collected and characterized by XRD and SEM to explore the effect mechanism of cations on the MgH_2 hydrolysis.

According to the XRD patterns in Fig. 3, the final MgH_2 hydrolysates in different chloride solutions are the corresponding cationic hydroxides. Among them, the hydrolysate in the $FeCl_3$ solution cannot be directly characterized by XRD due to a severe amorphization. After annealing at 650 ℃ in a nitrogen atmosphere, the XRD of Fe_2O_3 product indirectly confirms the presence of iron hydroxide in the hydrolysate. In addition, the XRD of hydrolysate in $CuCl_2$ solution shows the diffraction peaks of CuCl, which may be resulted from the incomplete hydrolysis of MgH_2. During the drying process of the hydrolysate, Cu (II) was redoxed to obtain Cu (I) by MgH_2. This phenomenon also appears in the hydrolysis products of $CuSO_4$ and

$Fe_2(SO_4)_3$, and the formation of Cu_2O and Fe_3O_4 phases also indicates the existence of this redox reaction (See Fig. S2 in supplementary material).

The H_2 generation rate is improved in the order of $Mg^{2+} < Zn^{2+} < Cu^{2+} < Fe^{3+}$, which is the same order as the thermodynamic tendency of hydroxide formation, i.e. the OH^- affinity of the cation. OH^- affinity is defined by the pK_{sp}/x value[28]. $pK_{sp}/x = -\lg K_{sp}/x$, K_{sp} is the solubility product of $M(OH)_x$, and x is the cation valence. Apparently, the cations with higher OH^- affinity display a stronger promotion effect on the hydrogen evolution (see Table 1).

Fig. 4 shows the SEM images of the hydrolysis products, which illustrate the different induction effect of M^{x+} on the hydrolysis of MgH_2. The hydrolysis reacts violently and quickly in $FeCl_3$ solution so that the MgH_2 particles changed a lot in appearance while the overall shape of the MgH_2 particles has not changed much in pure water and $MgCl_2$ solution (Fig. 4a-c). In addition, we can see from Fig. 4d-f that there is a clear passivate $Mg(OH)_2$ layer wrapped on the surface of MgH_2 particle in the pure water condition, but in the $MgCl_2$ solution, the $Mg(OH)_2$ sheets have a tendency to extend outward, and for the $FeCl_3$ solution, visible product particles with an average diameter ~100 nm can be observed with the disappearance of MgH_2 particles. In the $Fe_2(SO_4)_3$ solution, the morphology change of MgH_2 particles is showed in Fig. S4b, the MgH_2 particles also changed greatly in appearance and the final products are formed with lots of flakes showing a diffusion state (Fig. S4d). The change of the surface of MgH_2 particles in different solutions suggests that the cations play an important role in inducing the growth of the hydrolysis products for the solution to reach the MgH_2 surface. Moreover, the cations with higher affinity to OH^- will exhibit a stronger introducing effect, as the surface of MgH_2 particles has a more dramatic changes in appearance in $FeCl_3$ solution than in $MgCl_2$ solution.

Based on the SEM results, this promotion effect of various M^{x+} can be understood as the illustration in Fig. 5. Different from the passive $Mg(OH)_2$ formed in the MgH_2 surface in pure water (Fig. 5a), the M^{x+} existed in solution can induce the conformation of $M(OH)_x$ around the MgH_2 particles (Fig. 5b). In this case, the cations M^{x+} with high affinity to OH^- will compete for the OH^- species and induce the growth of $M(OH)_x$ with priority, so the formation of the $Mg(OH)_2$ passivation layer in the MgH_2 surface is inhibited and the hydrogen generation is enhanced to a large extend. The XRD characterizations of the precipitation product also fit the statement for the induction effect of cations very well.

3.2. The influence of anions in MgH_2 hydrolysis

The hydrolysis kinetic curves of different magnesium salt solutions are established in Fig. 6a. As can be seen, the presence of magnesium salts in the solution can obviously increase the hydrolysis rate compared to the pure water environment. $MgCl_2$, $MgSO_4$ and $Mg(CH_3COO)_2$ solution can achieve a high reaction degree to near 100% (1864.0 mL/g) within 150, 235 and 357 min, respectively. Nevertheless, the hydrolysis reaction degree is 70.0% (1304.8 mL/g) for $Mg(ClO_4)_2$ solution and 63.5% (1183.6 mL/g) for $Mg(NO_3)_2$ solution, even though the reaction time was increased to 400 min. It is distinctly that the improvement of MgH_2 hydrolysis is increased in this order of $MgCl_2$ > $MgSO_4$ > $Mg(CH_3COO)_2$ > $Mg(ClO_4)_2$ > $Mg(NO_3)_2$. Awad et al.[22] have reported that chloride ions can replace hydroxide ions which bring the formation of soluble $MgCl_2$ and the destruction of passive layer to promote the reaction. From our results, the various anions may have the similar function and the order of the replacement effect of anions is as follows: Cl^- > SO_4^{2-} > CH_3COO^- > ClO_4^- > NO_3^-. To further investigate the kinetics effect of Cl^-, the hydrogen generation of MgH_2 hydrolysis at various temperatures in $MgCl_2$ solution were obtained as shown in Fig. 6b. When the system temperature increased from 298 K to 328 K, the hydrogen yield of MgH_2 hydrolysis in $MgCl_2$ solution increased from 26.1% (298 K) to 45.3% (308 K), 72.0% (318 K) and 99.6% (328 K) in 20 min. And the apparent activation energy (E_a) was calculated by Eq. (2) to be 51.02 kJ mol^{-1}.

Besides the kinetics, it was found that the H_2O utilization rate is different in various anions solutions. Generally, the MgH_2 hydrolysis is carried out in a condition that the amount of H_2O is far exceeding in order to guarantee a complete hydrolysis of MgH_2, which inevitably leads to the decreased hydrogen capacity in the whole MgH_2/H_2O system. Obviously, it is significative to enhance the H_2O utilization, so we use the H_2O utilization rate to describe the roles of anions and the results are shown in Fig. 7 (Complete and specific hydrogen release curves are shown in Figure. S5-S8). Because of the low degree of hydrolysis, the $Mg(ClO_4)_2$ and $Mg(NO_3)_2$ solutions are not considered. For a single anion, the H_2O utilization rate is less than 32% (Fig. 7a). However, when two anions are mixed together, the H_2O utilization rate is improved as shown in Fig. 7b. Specially for the mixed $MgCl_2$ and $MgSO_4$ solution (0.5 M $MgCl_2$ + 0.1 M $MgSO_4$), the H_2O utilization rate comes to 43%. What's more, Fig. 7c indicates that the concentrations of the mixed solutions also affect the water utilization, and the 0.5 M $MgCl_2$ + 0.05 M $MgSO_4$ solution demonstrates the highest H_2O utilization rate of 47.9%.

Except for the influence of the concentration for the mixed solution, the volume of the solution also has a certain effect on the water utilization rate. The relationship between H_2O utilization rate and solution volume in 0.5 M $MgCl_2$ + 0.05 M $MgSO_4$ solution can be well described by the power function of Eq. (3), as shown by the black curve in Fig. 7d.

$$y = a \cdot x^b \quad (3)$$

This is a mathematical model to describe the trend of relationship changes, and has no actual physical and chemical meaning. However, on the grounds of this mathematical model, we designed a hydrogen evolution system as shown in Fig. 8a. It demonstrates that if there are 60 L (normal vehicle gasoline volume) mixed 0.5 M $MgCl_2$ + 0.05 M $MgSO_4$ solution in the system, the H_2O utilization rate will be 95.1%. On the other hand, if the weight of water is calculated, the systematic hydrogen capacity of MgH_2 hydrolysis process is 6.5 wt. %. The higher H_2O utilization rate will result in the higher systematic hydrogen capacity, and when the H_2O utilization rate comes to 100%, deservedly the hydrogen storage capacity of the MgH_2/H_2O system is 6.5 wt. %. In this regard, with the increased volume of 0.5 M $MgCl_2$ + 0.05 M $MgSO_4$ solution as displayed in Fig. 8b, which leads to an increased H_2O utilization rate, the hydrogen evolution system in Fig. 8a can gradually approaching 100% H_2O utilization rate which is established as a dashed line (Fig. 8b). In this way, the hydrogen storage capacity of the whole system can achieve the theoretical hydrogen storage capacity at the same time.

For the sake of exploring the mechanism of anion effect on water utilization, the morphology of the final products in various anions solutions is characterized as shown in Fig. 9. It can be seen that as the particle size of the flakes decreases, the hydrolysis efficiency increases significantly. The maximum water utilization rate obtained corresponds the smallest particle size distribution in the final products, which is mainly in the range of 40 - 60 nm (Fig. 9a). On the contrary, the minimum water utilization rate gives the largest particle size distribution of 500 - 600 nm (Fig. 9d). Furthermore, in the single anion solution, the particle size of product is even > 1 μm (Fig. S9). These results indicate that the anion solution does affect the water utilization rate by affecting the morphology of the hydrolysate. The larger the flaky size of the hydrolysate particles, the easier it is to form a flaky cross structure (Fig. 9c-d), and the easier it is to lock in moisture, thus reducing the utilization of water.

4. Conclusion

In this study, the functions of different anions and cations in solutions for MgH_2 hydrolysis are demonstrated and the H_2 generation from the MgH_2 hydrolysis is promoted significantly by low-cost chlorides and sulfates solutions. The cations with high affinity to OH^- in the solution will induce the outward growth of hydroxide and thus inhibiting the formation of the surface $Mg(OH)_2$ passivation layer. The H_2 yield of MgH_2 hydrolysis in $FeCl_3$ and $Fe_2(SO_4)_3$ solutions, in which the Fe^{3+} has the largest affinity to OH^- among the studied metal

cations, comes up to 1632.0 mL/g H_2 and 1664.0 mL/g in 6.2 min and 5 min, respectively. With regard to the anions, we found it can effectively affect the morphology of hydrolysis product, thereby affecting the water utilization. Especially in the mixed 0.5 M $MgCl_2$ and 0.05 M $MgSO_4$ solution, the H_2O utilization rate can reach to the highest value among the various anion solutions. Furthermore, under the prediction of the mathematical model for the relationship between H_2O utilization rate and solution volume, with continuously increasing the solution volume to 60 L, the H_2O utilization rate can reach to nearly 100%. On account of the high attainable hydrogen capacity and high abundance of the raw materials, the solution promoted hydrolysis of MgH_2 is highly attractive for onsite H_2 generation.

Acknowledgements

This work was partially supported by the National Key Research and Development Program of China (2017YFA0204600), the National Science Fund for Distinguished Young Scholars (51625102), the National Natural Science Foundation of China (51971065) and the Innovation Program of Shanghai Municipal Education Commission (2019–01–07–00–07-E00028). Zhenguo Huang is grateful for the financial support from ARC (DP170101773).

References

[1] S. Chu, A. Majumdar, Nature, 488 (2012) 294-303.

[2] N. Armaroli, V. Balzani, Angew. Chem. Int. Ed. Engl., 46 (2007) 52-66.

[3] L. Schlapbach, A. Zuttel, Nature, 414 (2001) 353-358.

[4] G.W. Crabtree, M.S. Dresselhaus, M.V. Buchanan, Phys. Today, 57 (2004) 39-44.

[5] X. Yu, Z. Tang, D. Sun, L. Ouyang, M. Zhu, Prog. Mater. Sci., 88 (2017) 1-48.

[6] T. He, H. Cao, P. Chen, Adv. Mater., 31 (2019) e1902757.

[7] X.L. Zhang, Y.F. Liu, X. Zhang, J.J. Hu, M.X. Gao, H.G. Pan, Mater. Today Nano, 9 (2020) 100064.

[8] W. Grochala, P.P. Edwards, Chem. Rev., 104 (2004) 1283-1316.

[9] J.G. Novakovic, N. Novakovic, S. Kurko, S.M. Govedarovic, T. Pantic, B.P. Mamula, K. Batalovic, J. Radakovic, J. Rmus, M. Shelyapina, N. Skryabina, P. de Rango, D. Fruchart, Chemphyschem, 20 (2019) 1216-1247.

[10] L. Ouyang, M. Ma, M. Huang, R. Duan, H. Wang, L. Sun, M. Zhu, Energies, 8 (2015) 4237-4252.

[11]T. Tayeh, A.S. Awad, M. Nakhl, M. Zakhour, J.F. Silvain, J.L. Bobet, Int. J. Hydrogen Energy, 39 (2014) 3109-3117.

[12]M. Tegel, S. Schöne, B. Kieback, L. Röntzsch, Int. J. Hydrogen Energy, 42 (2017) 2167-2176.

[13]H. Uesugi, T. Sugiyama, H. Nii, T. Ito, I. Nakatsugawa, J. Alloys Compd., 509 (2011) S650-S653.

[14]X. Xie, C. Ni, B. Wang, Y. Zhang, X. Zhao, L. Liu, B. Wang, W. Du, J. Alloys Compd., 816 (2020) 152634.

[15]J. Chen, H. Fu, Y. Xiong, J. Xu, J. Zheng, X. Li, Nano Energy, 10 (2014) 337-343.

[16]J. Jiang, L. Ouyang, H. Wang, J. Liu, H. Shao, M. Zhu, Chemphyschem, 20 (2019) 1316-1324.

[17]J.M. Huang, R.M. Duan, L.Z. Ouyang, Y.J. Wen, H. Wang, M. Zhu, Int. J. Hydrogen Energy, 39 (2014) 13564-13568.

[18]B. Yang, J. Zou, T. Huang, J. Mao, X. Zeng, W. Ding, Chem. Eng. J., 371 (2019) 233-243.

[19]L.Z. Ouyang, Z.J. Cao, H. Wanga, J.W. Liu, D.L. Sun, Q.A. Zhang, M. Zhu, J. Alloys Compd., 586 (2014) 113-117.

[20]J. Mao, J. Zou, C. Lu, X. Zeng, W. Ding, J. Power Sources, 366 (2017) 131-142.

[21]J.P. Tessier, P. Palau, J. Huot, R. Schulz, D. Guay, J. Alloys Compd., 376 (2004) 180-185.

[22]A.S. Awad, E. El-Asmar, T. Tayeh, F. Mauvy, M. Nakhl, M. Zakhour, J.L. Bobet, Energy, 95 (2016) 175-186.

[23]M.-H. Grosjean, L. Roué, J. Alloys Compd., 416 (2006) 296-302.

[24]M. Ma, L. Ouyang, J. Liu, H. Wang, H. Shao, M. Zhu, J. Power Sources, 359 (2017) 427-434.

[25]D. Gan, Y. Liu, J. Zhang, Y. Zhang, C. Cao, Y. Zhu, L. Li, Int. J. Hydrogen Energy, 43 (2018) 10232-10239.

[26]M. Huang, L. Ouyang, H. Wang, J. Liu, M. Zhu, Int. J. Hydrogen Energy, 40 (2015) 6145-6150.

[27]L.G. Sevastyanova, S.N. Klyamkin, B.M. Bulychev, Int. J. Hydrogen Energy, 45 (2019) 3046-3052.

[28]J. Zheng, D. Yang, W. Li, H. Fu, X. Li, Chem. Commun., 49 (2013) 9437-9439.

[29]M. Grosjean, M. Zidoune, L. Roue, J. Huot, Int. J. Hydrogen Energy, 31 (2006) 109-119.

Figure and table captions

Table 1 The pK_{sp}/x of cations and corresponding hydrogen evolution in different solutions.

Fig. 1. Schematic diagram of hydrolysis reaction device.

Fig. 2. Hydrolysis kinetic curves of the MgH_2 in different chloride solutions (a) and sulfate solutions (b) at 298 K. Hydrolysis kinetic curves of the MgH_2 at different temperatures in $Fe_2(SO_4)_3$ solution (c) and their Arrhenius plot (d).

Fig. 3. XRD patterns of MgH_2 hydrolysis products in (a) $MgCl_2$ solution; (b) $ZnCl_2$ solution; (c) $CuCl_2$ solution; (d) $FeCl_3$ solution.

Fig. 4. SEM images of the integrated MgH_2 particles in (a) pure water, (b) $MgCl_2$ solution and (c) $FeCl_3$ solution after 30 min reaction; the surface of MgH_2 particles in (d) pure water, (e) $MgCl_2$ solution and (f) $FeCl_3$ solution after 30 min reaction.

Fig. 5. Schematic illustration of the mechanism for the hydrolysis of MgH_2 in (a) pure water and (b) M^{x+} solution.

Fig. 6. (a) Hydrolysis kinetic curves of the MgH_2 in different Mg^{2+} solutions and pure water at 298 K. (b) Hydrolysis kinetic curves of the MgH_2 in $MgCl_2$ solution at different temperatures. The inset is their Arrhenius plot.

Fig. 7. The water utilization rate of MgH_2 hydrolysis in the (a) 0.5 M $MgCl_2$, $MgSO_4$ and $Mg(CH_3COO)_2$ solutions, and (b) the mixture solutions of 0.5 mol L^{-1} $MgCl_2$, 0.5 M $MgCl_2$ + 0.1 M $Mg(CH_3COO)_2$, 0.5 M $MgCl_2$ + 0.1 M $MgSO_4$, and (c) the mixed solutions of different concentration ratios for $MgCl_2$ and $MgSO_4$ at 298 K. The solution volume is 10 ml. (d) the power function model Eq. (3) fitting curve between H_2O utilization rate and solution volume for 0.5 M $MgCl_2$ + 0.05 M $MgSO_4$ solution.

Fig. 8. (a) Proposed hydrogen generation system based on the hydrolysis of MgH_2 in mixed 0.5 M $MgCl_2$ and 0.05 M $MgSO_4$ solution with continuous feeding of MgH_2; (b) The solid curve: simulated system H_2O utilization rate at different solution volume based on Eq. (3). The dashed line: the 100% H_2O utilization rate.

Fig. 9. SEM images of hydrolysis products in the mixed solutions of (a) 0.5 M $MgCl_2$ + 0.05 M $MgSO_4$, (b) 0.5 M $MgCl_2$ + 0.1 M $MgSO_4$, (c) 0.5 M $MgCl_2$ + 0.5 M $MgSO_4$, (d) 0.5 M $MgCl_2$ + 0.1 M $Mg(CH_3COO)_2$.

Table list:

Table 1. The pK_{sp}/x of cations and corresponding hydrogen evolution in different solutions.

Solution	pK_{sp}/x of cation	H_2 yield in 10 min[ml/g]
$Fe_2(SO_4)_3$	12.85	1664.0
$CuSO_4$	9.83	558.4
$ZnSO_4$	8.83	280.0
$MgSO_4$	5.62	127.1
$FeCl_3$	12.85	1632.0
$CuCl_2$	9.83	738.6
$ZnCl_2$	8.25	373.2
$MgCl_2$	5.62	227.0

Figure list:

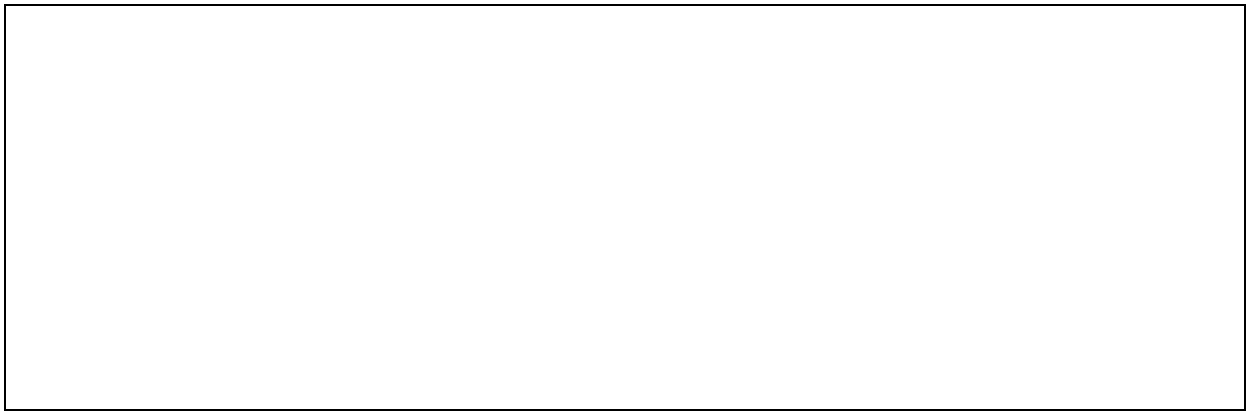

Fig. 1. Schematic diagram of hydrolysis reaction device.

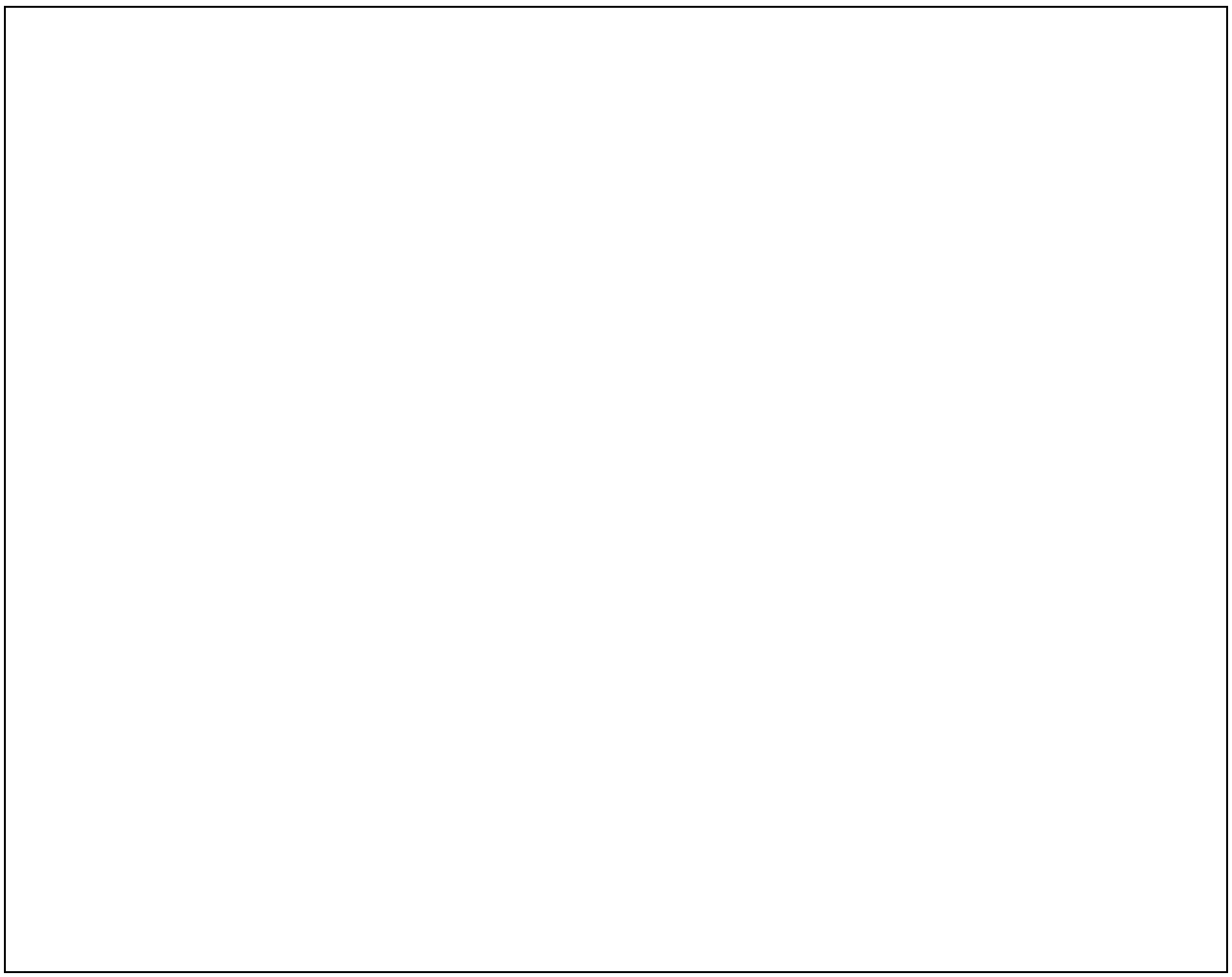

Fig. 2. Hydrolysis kinetic curves of the MgH_2 in different chloride solutions (a) and sulfate solutions (b) at 298 K. Hydrolysis kinetic curves of the MgH_2 at different temperatures in $Fe_2(SO_4)_3$ solution (c) and their Arrhenius plot (d).

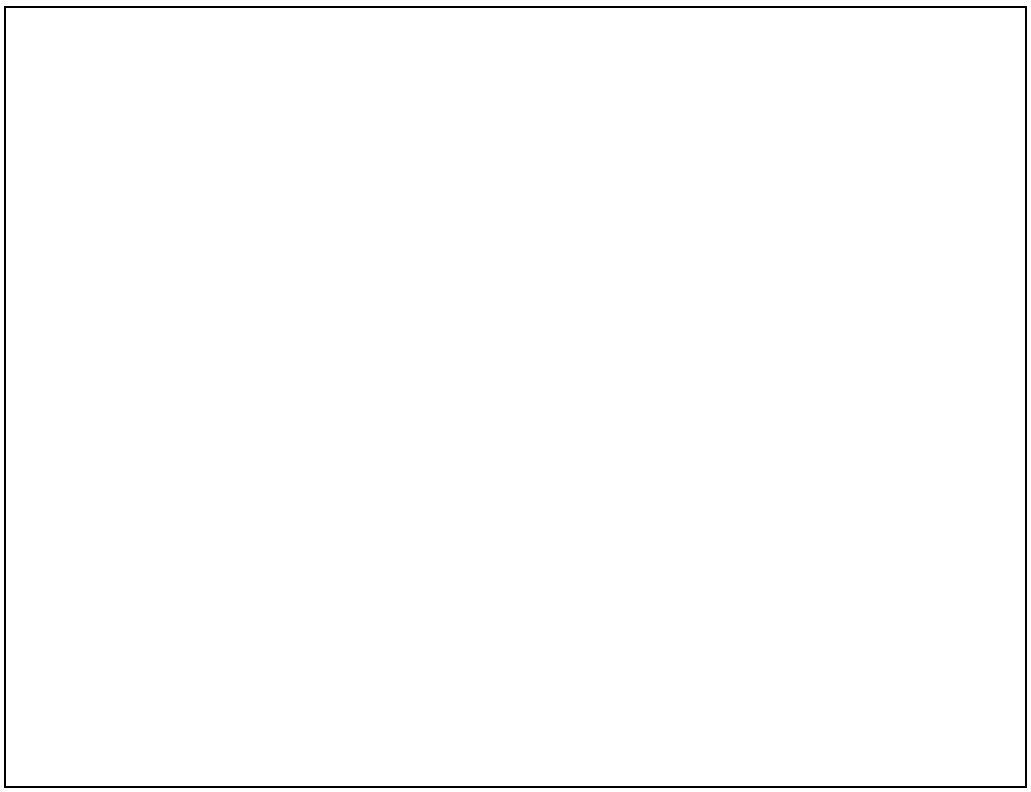

Fig. 3. XRD patterns of MgH_2 hydrolysis products in (a) $MgCl_2$ solution; (b) $ZnCl_2$ solution; (c) $CuCl_2$ solution; (d) $FeCl_3$ solution.

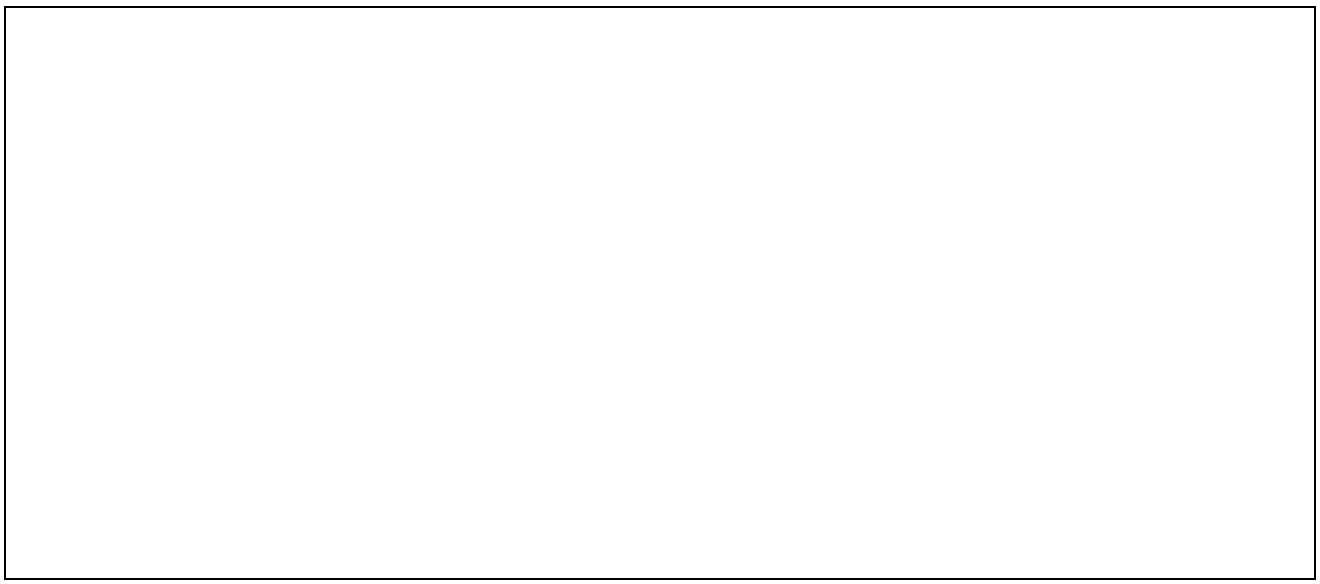

Fig. 4. SEM images of the integrated MgH_2 particles in (a) pure water, (b) $MgCl_2$ solution and (c) $FeCl_3$ solution after 30 min reaction; the surface of MgH_2 particles in (d) pure water, (e) $MgCl_2$ solution and (f) $FeCl_3$ solution after 30 min reaction.

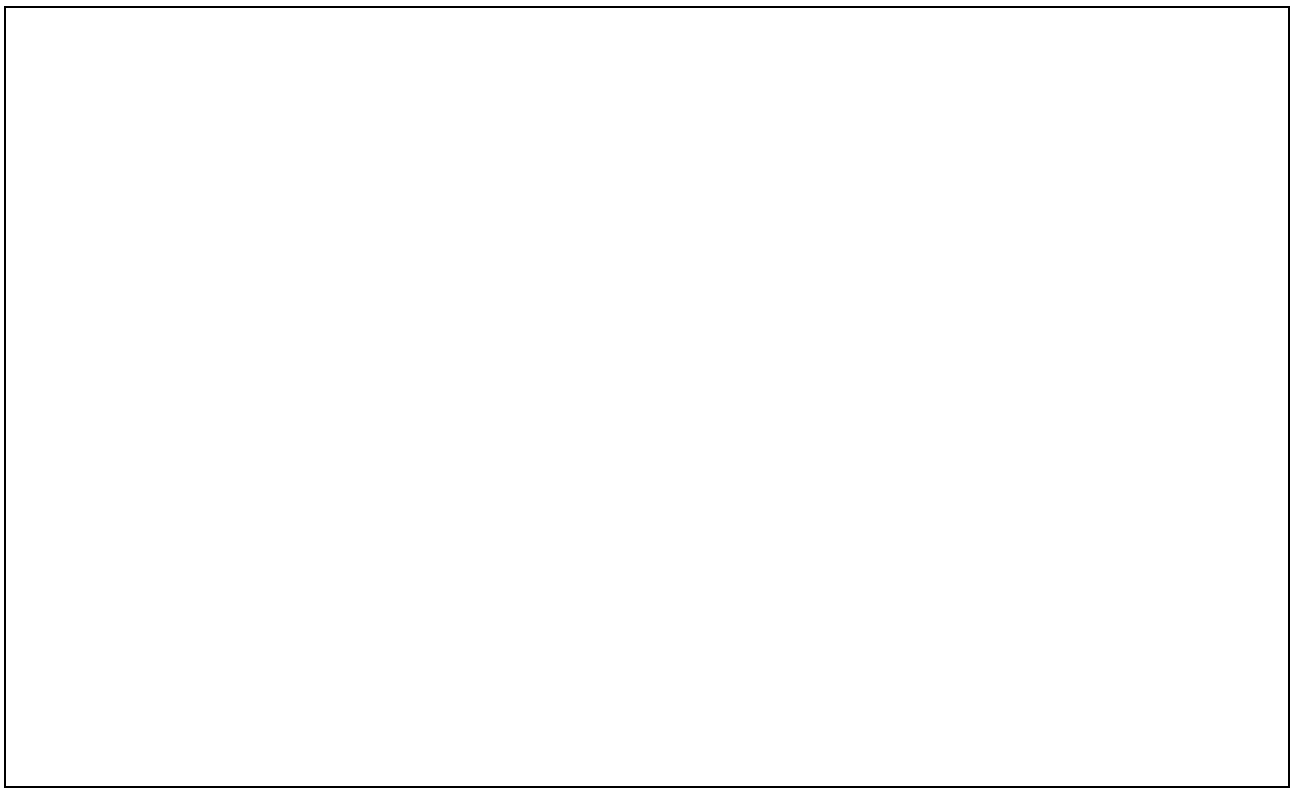

Fig. 5. Schematic illustration of the mechanism for the hydrolysis of MgH_2 in (a) pure water and (b) M^{x+} solution.

Fig. 6. (a) Hydrolysis kinetic curves of the MgH_2 in different Mg^{2+} solutions and pure water at 298 K. (b) Hydrolysis kinetic curves of the MgH_2 in $MgCl_2$ solution at different temperatures. The inset is their Arrhenius plot.

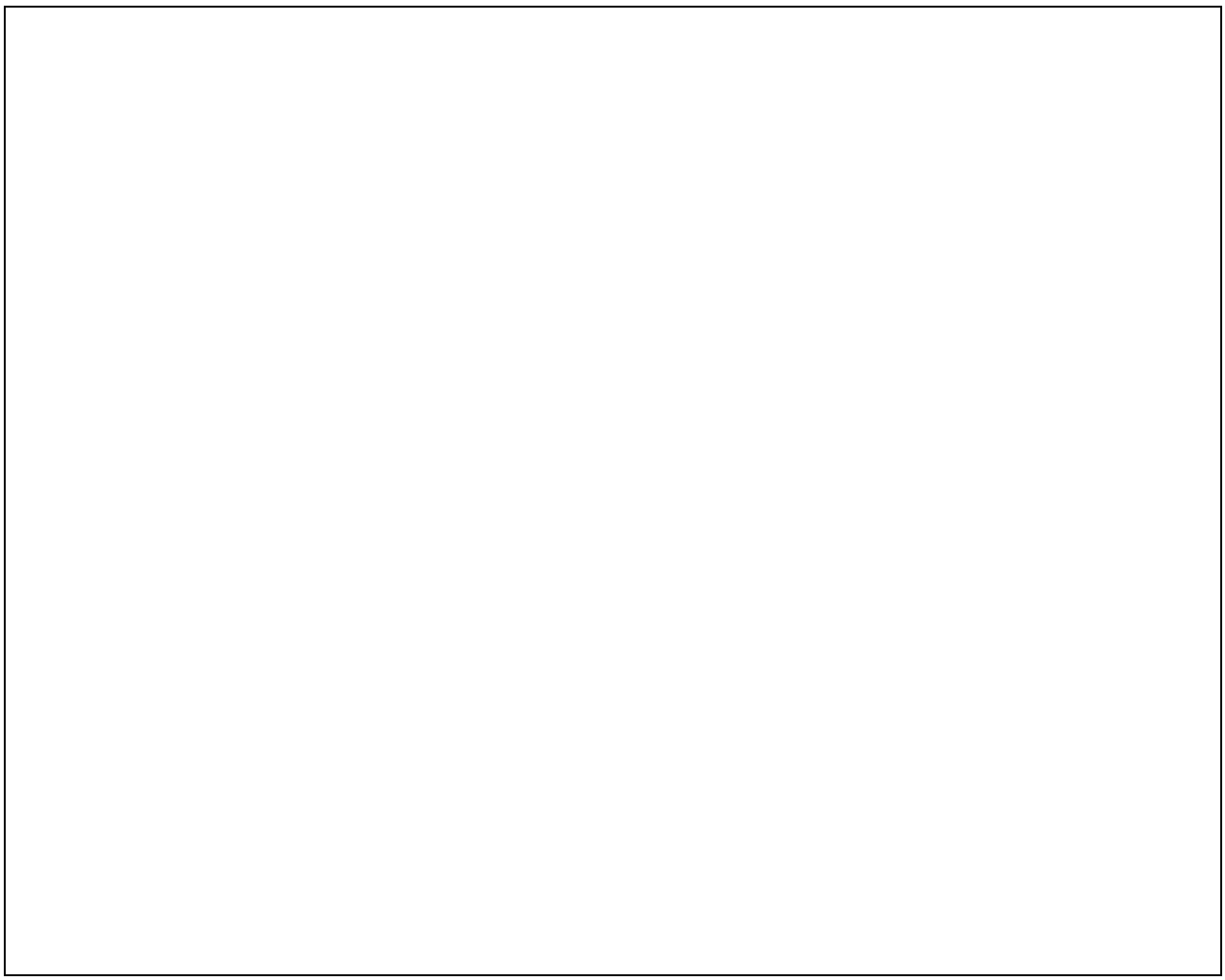

Fig. 7. The water utilization rate of MgH_2 hydrolysis in the (a) 0.5 M $MgCl_2$, $MgSO_4$ and $Mg(CH_3COO)_2$ solutions, and (b) the mixture solutions of 0.5 mol L^{-1} $MgCl_2$, 0.5 M $MgCl_2$ + 0.1 M $Mg(CH_3COO)_2$, 0.5 M $MgCl_2$ + 0.1 M $MgSO_4$, and (c) the mixed solutions of different concentration ratios for $MgCl_2$ and $MgSO_4$ at 298 K. The solution volume is 10 ml. (d) the power function model Eq. (3) fitting curve between H_2O utilization rate and solution volume for 0.5 M $MgCl_2$ + 0.05 M $MgSO_4$ solution.

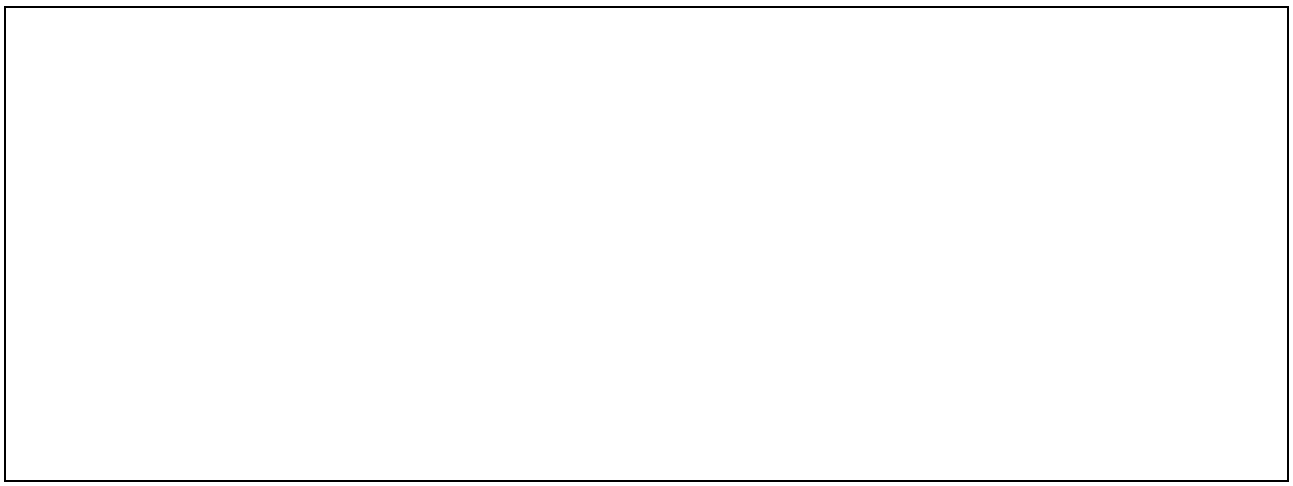

Fig. 8. (a) Proposed hydrogen generation system based on the hydrolysis of MgH_2 in mixed 0.5 M $MgCl_2$ and 0.05 M $MgSO_4$ solution with continuous feeding of MgH_2; (b) The solid curve: simulated system H_2O utilization rate at different solution volume based on Eq. (3). The dashed line: the 100% H_2O utilization rate.

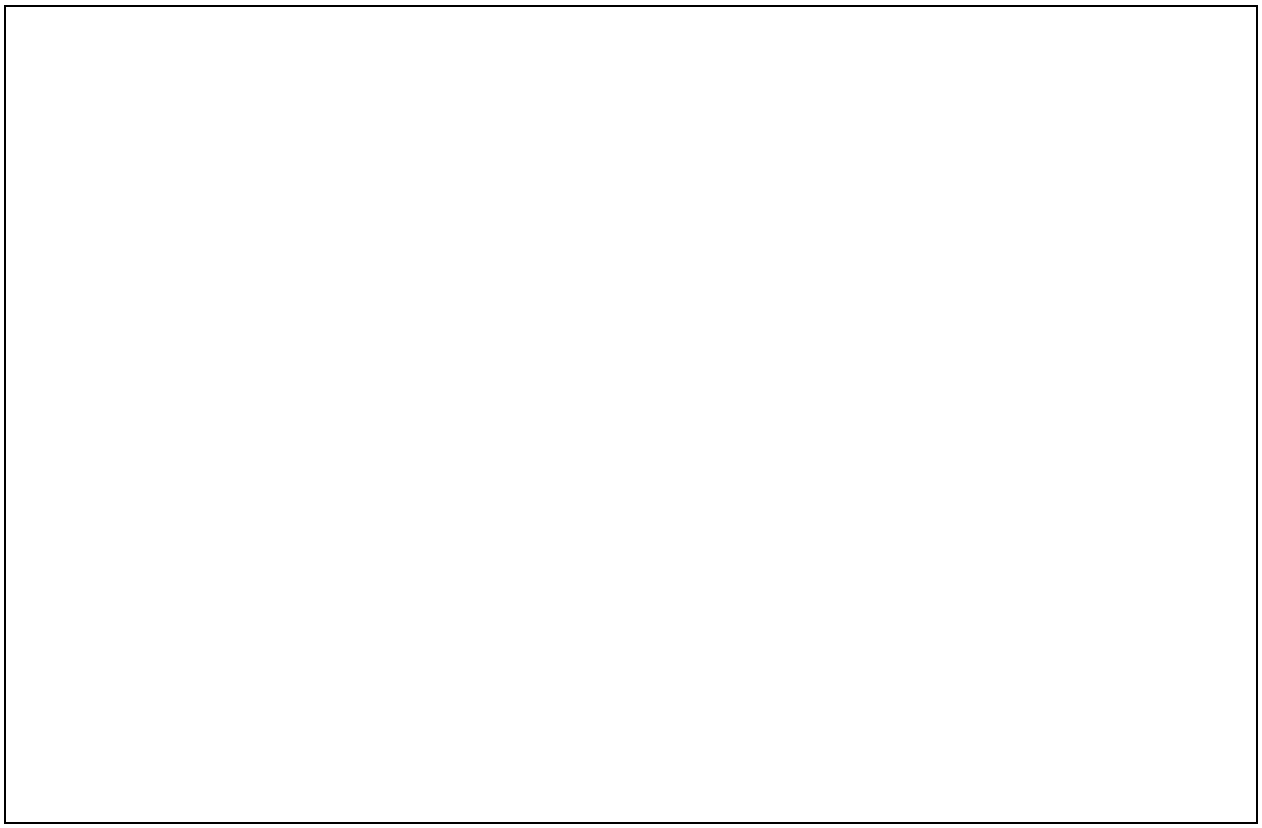

Fig. 9. SEM images of hydrolysis products in the mixed solutions of (a) 0.5 M $MgCl_2$ + 0.05 M $MgSO_4$, (b) 0.5 M $MgCl_2$ + 0.1 M $MgSO_4$, (c) 0.5 M $MgCl_2$ + 0.5 M $MgSO_4$, (d) 0.5 M $MgCl_2$ + 0.1 M $Mg(CH_3COO)_2$.